Application of Trajectory Optimization Method for a Space Manipulator with Four Degrees of Freedom

Tomasz Rybus[1], Karol Seweryn[1] and Jurek Z. Sąsiadek[2]
[1]*Space Research Centre (CBK PAN), Bartycka 18a, Warsaw, Poland*
[2]*Department of Mechanical and Aerospace Eng., Carleton University, Ottawa, Ontario, Canada*

Keywords: Space Robotics, Free-floating Space Manipulator, Trajectory Optimization, On-orbit Servicing.

Abstract: Planned active debris removal and on-orbit servicing missions require capabilities for capturing objects on Earth's orbit, e.g., by the use of a manipulator. In this paper we demonstrate the application of a trajectory optimization algorithm for free-floating satellite-manipulator systems in two cases: a planar system with 2 degrees of freedom manipulator and a spatial system with a manipulator having four degrees of freedom. For the case with planar system, results of experiments performed on an air-bearing microgravity simulator are shown. Quadratic norm connected with the power consumption of manipulator motors has been used as a cost functional that is minimized. Optimal trajectories are compared with straight-line trajectories and it is shown that the optimization allows reduction of the power use of manipulator motors (for the planar system 30 trajectories based on randomly selected initial and final end-effector positions were analysed and the cost functional was, on average, reduced by 49.4%). The presented method could be modified by using cost functional that would, e.g., minimize disturbance on the satellite.

1 INTRODUCTION

Capabilities for capturing objects on Earth's orbit by unmanned satellites are required in planned active debris removal and on-orbit servicing missions. European Space Agency (ESA) is studying the concept of active debris removal to prevent predicted growth of space debris population on Low Earth Orbit. Studies show that current debris population is likely to increase due to collisions between existing space debris (Liou, Johnson, and Hill, 2010). Thus, removal of large intact objects from orbit might be necessary in the coming years. On-orbit servicing missions are proposed to prolong the operational lifetime of satellites. Repairing satellite with unmanned servicing vehicle could be economically feasible (Sullivan and Akin, 2012). Specific active debris removal and on-orbit servicing missions have been proposed in recent years, e.g., by Hausmann et al. (2015). Many of the proposed mission concepts rely on the use of a manipulator for performing capture manoeuvre.

Design of a manipulator for orbital operations is a challenging task, since such manipulators are complex mechatronic systems that must operate in space environment and must have a very low mass. Control of a satellite-manipulator system during capture manoeuvre is also one of the major challenges in on-orbit servicing. The motion of the manipulator influences both the position and the orientation of the manipulator-equipped satellite. This effect must be taken into account during manipulator trajectory planning and control. Reaction torques and forces induced by the motion of the manipulator must either be fully compensated by the guidance, navigation and control subsystem (GNC) of the satellite or this subsystem must be switched off during the manoeuvre. In the latter case, the satellite is in free-floating state (Dubowsky and Papadopoulos, 1993).

In our study we focus on the subject of end-effector trajectory planning for a free-floating manipulator. Methods that allow optimization of planned trajectory are especially interesting and several approaches to optimal trajectory planning and control were developed in the last decade, e.g., by Aghili (2008) and Flores-Abad et al. (2014a). Another benefit of optimization techniques is that they could also be used to minimize manipulator disturbances on the manipulator-equipped satellite (Kaigom, Jung and Rossmann, 2011). The broad review of on-orbit servicing technologies presented

Rybus, T., Seweryn, K. and Sąsiadek, J.
Application of Trajectory Optimization Method for a Space Manipulator with Four Degrees of Freedom.
DOI: 10.5220/0005981000920101
In *Proceedings of the 13th International Conference on Informatics in Control, Automation and Robotics (ICINCO 2016) - Volume 1*, pages 92-101
ISBN: 978-989-758-198-4

by Flores-Abad et al. (2014b) includes a section devoted to trajectory planning. In our paper we follow the approach for optimal trajectory planning that was proposed by Seweryn and Banaszkiewicz (2008). This approach is based on the Generalized Jacobian Matrix (GJM), introduced by Umetani and Yoshida (1989) for systems with zero linear and angular momentum. Seweryn and Banaszkiewicz extended GJM for systems with non-zero and not-conserved linear and angular momentum (e.g., with additional forces from thrusters acting on the satellite during the realization of the end-effector trajectory). They proposed an optimization algorithm that is based on the calculus of variations. The cost functional trades off for power use of motors in the manipulator joints as well as for additional conditions constraining the end-effector motion. Rybus, Seweryn and Sąsiadek (2016) presented several improvements to this algorithm, the most important being the modification of the boundary conditions of the optimization problem to allow imposing constraints for the end-effector velocity. During the capture manoeuvre the end-effector velocity at the moment of grasping must match the velocity of the grasping point on the target satellite; thus, it is required to define the final end-effector velocity during the trajectory optimization. The original algorithm was also extended to include the time of the manipulator motion as a parameter that is optimized. As a result, it is possible to compute the optimal time for the capture manoeuvre. The trajectory optimization algorithm is suitable for a general case of a manipulator with n degrees of freedom, but Rybus, Seweryn and Sąsiadek (2016) illustrated the presentation of their algorithm with only a simple example (i.e. a planar manipulator with 2 degrees of freedom).

In this paper we demonstrate the use of the aforementioned algorithm for the optimization of end-effector trajectory of a spatial manipulator with 4 degrees of freedom, mounted on a free-floating satellite. As torques required to position the end-effector are much higher than torques needed for obtaining the desired end-effector orientation, we do not consider the optimization of end-effector orientation. In the presented numerical example we use mass and geometrical properties of the prototype robotic arm WMS1 LEMUR presented by Seweryn et al. (2014). WMS1 LEMUR has 7 degrees of freedom: four joints are responsible for obtaining the end-effector position (one joint is redundant) and three joints are responsible for obtaining the end-effector orientation. In this study we use the trajectory planning algorithm for the first four joints.

Demonstrating that the optimization method proposed by Seweryn and Banaszkiewicz (2008) and extended by Rybus, Seweryn and Sąsiadek (2016) can be successfully used for a real spatial manipulator is the main contribution of this paper. Following Rybus and Seweryn (2015), we also present the results of an experimental study, in which trajectory optimization was performed for a real planar free-floating system with a manipulator with 2 degrees of freedom. The planar air-bearing microgravity simulator described by Rybus et al. (2013) was used for this purpose. In order to assess the advantages of the optimization algorithm in this simplified planar case we compared the optimal trajectory with a straight-line trajectory for 30 randomly selected initial and final positions of the end-effector.

The paper is organized as follows. In Section 2, equations describing the dynamics of a free-floating satellite-manipulator system are presented, while the trajectory optimization algorithm is shown in Section 3. Equations contained in these two sections were earlier presented by Rybus, Seweryn and Sąsiadek (2016). The results of experiments performed on the microgravity simulator are shown in Section 4. Application of the optimization algorithm for the manipulator with 4 degrees of freedom is presented in Section 5. Discussion is presented in Section 6 and the paper concludes with Section 7.

2 FREE-FLOATING SATELLITE-MANIPULATOR SYSTEMS

A free-floating satellite equipped with a manipulator with n degrees of freedom is presented in Fig. 1, where coordinate systems and selected geometrical parameters of the satellite-manipulator system are shown. In this section we follow the approach presented by Seweryn and Banaszkiewicz (2008) and by Rybus, Seweryn and Sąsiadek (2016).

All equations are expressed in the inertial reference frame (denoted as CS_{ine} in Fig. 1). The end-effector position is expressed as:

$$\mathbf{r}_{ee} = \mathbf{r}_s + \mathbf{r}_q + \sum_{i=1}^{n} \mathbf{l}_i \,, \tag{1}$$

where $\mathbf{r}_s$ is the position of the satellite center of mass, $\mathbf{r}_q$ is the position of the first kinematic pair of the manipulator with respect to the satellite, and $\mathbf{l}_i$ is

the position of the *i+1* kinematic pair in respect to the *i*th kinematic pair.

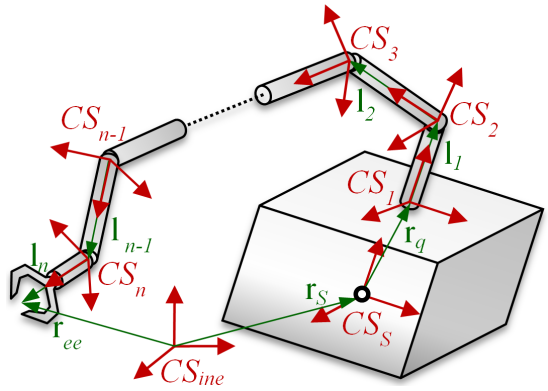

Figure 1: A schematic view of the satellite-manipulator system.

End-effector linear and angular velocities are given by the following equation:

$$\begin{bmatrix} \mathbf{v}_{ee} \\ \boldsymbol{\omega}_{ee} \end{bmatrix} = \mathbf{J}_S \begin{bmatrix} \mathbf{v}_S \\ \boldsymbol{\omega}_S \end{bmatrix} + \mathbf{J}_M \dot{\boldsymbol{\theta}}, \tag{2}$$

where:

$$\mathbf{J}_S = \begin{bmatrix} \mathbf{I} & \tilde{\mathbf{r}}_{ee\_s}^T \\ \mathbf{0} & \mathbf{I} \end{bmatrix}, \tag{3}$$

$$\mathbf{J}_M = \begin{bmatrix} \mathbf{k}_1 \times (\mathbf{r}_{ee} - \mathbf{r}_1) & \cdots & \mathbf{k}_n \times (\mathbf{r}_{ee} - \mathbf{r}_n) \\ \mathbf{k}_1 & \cdots & \mathbf{k}_n \end{bmatrix} \tag{4}$$

In the above equations $\mathbf{v}_S$ and $\boldsymbol{\omega}_S$ are the linear and angular velocities of the satellite, $\dot{\boldsymbol{\theta}}$ is the *n*-dimensional vector containing angular velocities of the manipulator joints, $\mathbf{J}_S$ is the Jacobian of the satellite (6 x 6 matrix), while $\mathbf{J}_M$ is the standard Jacobian of a non-space manipulator expressed in the inertial reference frame (6 x *n* matrix), $\mathbf{I}$ denotes the identity matrix, $\mathbf{0}$ denotes the zero matrix, $\mathbf{r}_{ee\_s} = \mathbf{r}_{ee} - \mathbf{r}_s$, ~ denotes a matrix which is equivalent of a vector cross-product, $\mathbf{k}_i$ and $\mathbf{r}_i$ are the unit vector of angular velocity and the position of the *i*th kinematic pair, respectively. The angular momentum of the satellite-manipulator system can be expressed as:

$$\mathbf{L} = \mathbf{L}_0 + \mathbf{r}_s \times \mathbf{P}, \tag{5}$$

where $\mathbf{L}_0$ is the initial angular momentum of the system. The momentum $\mathbf{P}$ and the angular momentum of the satellite-manipulator system are given by the following equation:

$$\begin{bmatrix} \mathbf{P} \\ \mathbf{L}_0 + \mathbf{r}_s \times \mathbf{P} \end{bmatrix} = \mathbf{H}_2 \begin{bmatrix} \mathbf{v}_s \\ \boldsymbol{\omega}_s \end{bmatrix} + \mathbf{H}_3 \dot{\boldsymbol{\theta}} = \begin{bmatrix} \mathbf{f}_m \\ \mathbf{f}_{am} \end{bmatrix}, \tag{6}$$

where:

$$\mathbf{H}_2 = \begin{bmatrix} \mathbf{A} & \mathbf{B} \\ \mathbf{B}^T + \tilde{\mathbf{r}}_s \mathbf{A} & \mathbf{E} + \tilde{\mathbf{r}}_s \mathbf{B} \end{bmatrix} \tag{7}$$

$$\mathbf{H}_3 = \begin{bmatrix} \mathbf{D} \\ \mathbf{F} + \tilde{\mathbf{r}}_s \mathbf{D} \end{bmatrix} \tag{8}$$

Here it should be noted that the matrices $\mathbf{H}_2$ i $\mathbf{H}_3$ are influenced not only by the state of the manipulator, but also by the state of the satellite. The submatrices $\mathbf{A}$, $\mathbf{B}$, $\mathbf{D}$, $\mathbf{E}$ and $\mathbf{F}$ are defined as:

$$\mathbf{A} = \left(m_s + \sum_{i=1}^{n} m_i \right) \mathbf{I}, \tag{9}$$

$$\mathbf{B} = \left(m_s + \sum_{i=1}^{n} m_i \right) \tilde{\mathbf{r}}_{s\_q}, \tag{10}$$

$$\mathbf{D} = \sum_{i=1}^{n} m_i \mathbf{J}_{Ti}, \tag{11}$$

$$\mathbf{E} = \mathbf{I}_s + \sum_{i=1}^{n} \left(\mathbf{I}_i + m_i \tilde{\mathbf{r}}_{i\_s}^T \tilde{\mathbf{r}}_{i\_s} \right), \tag{12}$$

$$\mathbf{F} = \sum_{i=1}^{n} \left(\mathbf{I}_i \mathbf{J}_{Ri} + m_i \tilde{\mathbf{r}}_{i\_s} \mathbf{J}_{Ti} \right), \tag{13}$$

where $\mathbf{r}_{s\_q} = \mathbf{r}_s - \mathbf{r}_q$ and $\mathbf{r}_{i\_s} = \mathbf{r}_i - \mathbf{r}_s$, m_s and $\mathbf{I}_s$ are the mass and inertia matrix of the satellite, respectively, m_i and $\mathbf{I}_i$ are the mass and inertia matrix of *i*th manipulator link, respectively, $\mathbf{J}_{Ti}$ is the translational component of the manipulator Jacobian $\mathbf{J}_M$, while $\mathbf{J}_{Ri}$ is the rotational component of this Jacobian. In a free-floating system, the linear and the angular momentum are usually assumed as zero. Such assumption was taken, e.g., by Dubowsky and Papadopoulos (1993), Umetani and Yoshida (1989), and Lindberg, Longman, and Zedd (1993). However, in the approach introduced by Seweryn and Banaszkiewicz (2008) and presented herein, the momentum and angular momentum are not equal to zero. Instead, in eqn. (6) the momentum and the angular momentum are described by the time dependent functions $\mathbf{f}_m$ and $\mathbf{f}_{am}$ defined as: $\mathbf{f}_m = \int \mathbf{F}_s dt$ and $\mathbf{f}_{am} = \int \mathbf{H}_s + \tilde{\mathbf{r}}_s \mathbf{F}_s dt$, where $\mathbf{F}_s$ and $\mathbf{H}_s$ are forces and torques acting on the satellite. These could be forces and torques generated by the satellite

manoeuvring thrusters or external disturbances (e.g., forces and torques resulting from the gravity gradient).

The end-effector velocity is:

$$\begin{bmatrix}\mathbf{v}_{ee}\\ \boldsymbol{\omega}_{ee}\end{bmatrix}=\mathbf{J}_s\mathbf{H}_2^{-1}\begin{bmatrix}\mathbf{f}_m\\ \mathbf{f}_{am}\end{bmatrix}+\left(\mathbf{J}_M-\mathbf{J}_s\mathbf{H}_2^{-1}\mathbf{H}_3\right)\dot{\boldsymbol{\theta}}. \quad (14)$$

The following equation relates the angular velocities of joints with end-effector velocity in the CS_{ine}:

$$\dot{\boldsymbol{\theta}}=\left(\mathbf{J}_M-\mathbf{J}_s\mathbf{H}_2^{-1}\mathbf{H}_3\right)^{-1}\left(\begin{bmatrix}\mathbf{v}_{ee}\\ \boldsymbol{\omega}_{ee}\end{bmatrix}-\mathbf{J}_s\mathbf{H}_2^{-1}\begin{bmatrix}\mathbf{f}_m\\ \mathbf{f}_{am}\end{bmatrix}\right) \quad (15)$$

The satellite velocity is given by:

$$\begin{bmatrix}\mathbf{v}_s\\ \boldsymbol{\omega}_s\end{bmatrix}=\mathbf{H}_2^{-1}\left(\begin{bmatrix}\mathbf{f}_m\\ \mathbf{f}_{am}\end{bmatrix}-\mathbf{H}_3\dot{\boldsymbol{\theta}}\right). \quad (16)$$

As in (Seweryn and Banaszkiewicz, 2008) and (Rybus, Seweryn and Sąsiadek, 2016), we use Langrangian formalism to derive dynamics equations for the system. For the considered case of a system free-floating in space, the potential energy is neglected. We use the generalized coordinates (Junkins and Schaub, 1997):

$$\mathbf{q}_p=\begin{bmatrix}\mathbf{r}_s & \boldsymbol{\Theta}_s & \boldsymbol{\theta}\end{bmatrix}^T, \quad (17)$$

where $\boldsymbol{\Theta}_s$ is the orientation of the satellite. Following Seweryn and Banaszkiewicz (2008) we describe the orientation of the satellite by Euler angles, as their use is more intuitive and straightforward than the use of quaternions or orientation matrices. In the range of motion considered herein, the risk of obtaining singular configuration is very limited (there is no tumbling motion of the manipulator-equipped satellite). The Lagrange equation is:

$$\frac{d}{dt}\left(\frac{\partial\mathbf{T}}{\partial\dot{\mathbf{q}}}\right)-\frac{\partial\mathbf{T}}{\partial\mathbf{q}}=\mathbf{Q}, \quad (18)$$

where $\mathbf{T}$ is the kinetic energy of the system expressed as:

$$\mathbf{T}=\frac{1}{2}\begin{bmatrix}\mathbf{v}_s\\ \boldsymbol{\omega}_s\\ \dot{\boldsymbol{\theta}}\end{bmatrix}^T\begin{bmatrix}\mathbf{A} & \mathbf{B} & \mathbf{D}\\ \mathbf{B}^T & \mathbf{E} & \mathbf{F}\\ \mathbf{D}^T & \mathbf{F}^T & \mathbf{N}\end{bmatrix}\begin{bmatrix}\mathbf{v}_s\\ \boldsymbol{\omega}_s\\ \dot{\boldsymbol{\theta}}\end{bmatrix}, \quad (19)$$

and $\mathbf{Q}$ is the vector of generalized forces:

$$\mathbf{Q}=\begin{bmatrix}\mathbf{F}_s & \mathbf{H}_s & \mathbf{u}\end{bmatrix}^T, \quad (20)$$

where $\mathbf{u}$ is the control vector composed of driving torques in manipulator joints. In eqn. (19) the $\mathbf{N}$ matrix is given by:

$$\mathbf{N}=\sum_{i=1}^{n}\left(\mathbf{J}_{Ri}^T\mathbf{I}_i\mathbf{J}_{Ri}+m_i\mathbf{J}_{Ti}^T\mathbf{J}_{Ti}\right), \quad (21)$$

Equation (18) is used to derive the generalized equations of motion for the satellite-manipulator system:

$$\mathbf{Q}=\mathbf{M}\left(\mathbf{q}_p\right)\ddot{\mathbf{q}}_p+\mathbf{C}\left(\dot{\mathbf{q}}_p,\mathbf{q}_p\right)\dot{\mathbf{q}}_p, \quad (22)$$

where $\mathbf{M}$ denotes the mass matrix expressed as:

$$\mathbf{M}\left(\mathbf{q}_p\right)=\begin{bmatrix}\mathbf{A} & \mathbf{B} & \mathbf{D}\\ \mathbf{B}^T & \mathbf{E} & \mathbf{F}\\ \mathbf{D}^T & \mathbf{F}^T & \mathbf{N}\end{bmatrix}, \quad (23)$$

while $\mathbf{C}$ is the Coriolis Matrix with components given by:

$$\mathbf{C}_{ij}=\sum_{k=1}^{n}\left(\frac{d}{dq_k}m_{ij}-\frac{1}{2}\frac{d}{dq_i}m_{jk}\right), \quad (24)$$

where $m_{ij}\in\mathbf{M}\left(\mathbf{q}_p\right)$ and $i,j,k=1\ldots n$.

In eqn. (22) there are no potential forces, as the considered system is the state of free fall. Equation (22) can be used to determine the control vector $\mathbf{u}(t)$

3 TRAJECTORY OPTIMIZATION

The approach to the end-effector trajectory optimization that we use in our study was presented by Seweryn and Banaszkiewicz (2008), with improvements introduced by Rybus, Seweryn and Sąsiadek (2016) to enhance the capabilities of the algorithm. The optimization problem is how to drive the end-effector from its initial state to the desired final state while minimizing the optimization criterion.

The general form of the optimized functional G is:

$$G\left(\mathbf{q}_{vp}(t),\mathbf{u}(t),t\right)=$$

$$\int_{t_0}^{t_f}\left[L\left(\mathbf{q}_{vp}(t),\mathbf{u}(t),t\right)+\boldsymbol{\lambda}_{vp}(t)^T\,\mathbf{g}\left(\mathbf{q}_{vp}(t),\mathbf{u}(t),t\right)\right]dt, \quad (25)$$

where $\mathbf{q}_{vp}=[\mathbf{q}_v\ \mathbf{q}_p]^{\mathrm{T}}$, $\mathbf{q}_v=\frac{d\mathbf{q}_p}{dt}$, $\boldsymbol{\lambda}_{vp}=[\boldsymbol{\lambda}_v\ \boldsymbol{\lambda}_p]^{\mathrm{T}}$, $\boldsymbol{\lambda}_p$ and $\boldsymbol{\lambda}_v$ denotes the Lagrange multipliers associated with $\mathbf{q}_p$ and $\mathbf{q}_v$, respectively, while the function $\mathbf{g}$ describes the direct dynamics of the satellite-manipulator system:

$$\mathbf{g} = \begin{bmatrix} \dot{\mathbf{q}}_v \\ \dot{\mathbf{q}}_p \end{bmatrix} = \begin{bmatrix} \mathbf{M}^{-1}(\mathbf{Q} - \mathbf{C}\mathbf{q}_v) \\ \mathbf{q}_v \end{bmatrix}. \quad (26)$$

In eqn. (25) L is the cost functional to be minimized. The selection of the appropriate cost functional is not simple. This selection should be performed by a control engineer for the specific mission, taking into account the limitations and conditions defined for this mission. In papers related to space robotics, a criterion that assures minimization of changes of the satellite orientation is most commonly used, e.g., by Kaigom, Jung and Rossmann (2011), as any substantial changes of the satellite attitude should be avoided during the capture manoeuvre. However, some authors also take into account the power use of manipulator motors, e.g., Shah et al. (2013). In our study we follow the approach of Seweryn and Banaszkiewicz (2008) and we use quadratic norm of the control input as a cost functional:

$$L = \frac{1}{2}\mathbf{u}^T\mathbf{u}. \quad (27)$$

Such a simple cost functional, related to the power use of manipulator motors, is very common in automation and robotic. The presented method could easily be modified by using more complex cost functional that would allow for achievement of different goal. The Hamiltonian of the system is given by:

$$H = L + \boldsymbol{\lambda}_{vp}^T\mathbf{g}. \quad (28)$$

The extremum of G is found for:

$$\frac{\partial H}{\partial \mathbf{u}} = 0. \quad (29)$$

From eqn. (29), the control vector $\mathbf{u}$ can be computed. We define a state vector as:

$$\mathbf{x} = \begin{bmatrix} \mathbf{q}_v & \mathbf{q}_p & \boldsymbol{\lambda}_v & \boldsymbol{\lambda}_p \end{bmatrix}^T, \quad (30)$$

and obtain a set of $2(12 + 2n)$ differential equations that minimize the functional G and satisfy the boundary conditions:

$$\begin{bmatrix} \dot{\mathbf{q}}_{vp} \\ \dot{\boldsymbol{\lambda}}_{vp} \end{bmatrix} = \begin{bmatrix} \mathbf{g} \\ -\frac{\partial L}{\partial \mathbf{q}_{vp}} - \boldsymbol{\lambda}_{vp}^T\frac{\partial \mathbf{g}}{\partial \mathbf{q}_{vp}} \end{bmatrix}. \quad (31)$$

A Boundary Value Problem (BVP) is formulated and a set of eqn. (31) is solved with $2(12 + 2n)$ boundary conditions and 12 additional equations, which must be satisfied by the BVP solver. The initial state of the system ($\mathbf{q}_{vp}$ at the initial time t_0) is determined by the first $12 + 2n$ boundary conditions, while the values of Lagrange multipliers at the final time t_f are determined by another $12 + 2n$ equations. These Lagrange multipliers are calculated from the following equation:

$$\boldsymbol{\lambda}_{vp}(t_f) = \left(\mathbf{v}^T \frac{\partial \boldsymbol{\psi}}{\partial \mathbf{q}_{vp}} \right)_{t=t_f}, \quad (32)$$

Where the function $\boldsymbol{\psi}$ describes the final desired state of the end-effector ($\boldsymbol{\psi} = [\mathbf{r}_{ee}\ \boldsymbol{\Theta}_{ee}\ \mathbf{v}_{ee}\ \boldsymbol{\omega}_{ee}]^T$). Additional 12 parameters $\mathbf{v}$ are determined by the algorithm to satisfy equations for $\boldsymbol{\psi}$.

4 APPLICATION OF THE OPTIMIZATION ALGORITHM FOR A PLANAR MANIPULATOR WITH 2 DEGREES OF FREEDOM

To demonstrate the trajectory optimization algorithm, we performed an experiment on the planar air-bearing microgravity simulator described by Rybus et al. (2013). This simulator is a test-bed that allows for experimental validation of trajectory planning and control algorithms for free-floating satellite-manipulator systems. In this test-bed, a model of a satellite-manipulator system is mounted on planar air-bearings that allow almost frictionless motion on a $2x3m^2$ granite plate. Thus, microgravity conditions are simulated in two dimensions. Currently, a satellite model equipped with a manipulator with 2 degrees of freedom is operated on this testbed. Its parameters are summarized in Tab. 1. A detailed description of the experiment performed on the planar air-bearing microgravity simulator was presented by Rybus and Seweryn (2015). In the performed experiment at the initial time t_0 the velocities of manipulator joints and the velocity of the satellite are zero, thus the initial velocity of the end-effector is also zero. The desired final end-effector position is set $0.3m$ away from the initial position. The final end-effector velocity must be zero. The time of motion is set to $5s$.

For the planar system equipped with a manipulator with 2 degrees of freedom the solution that minimizes the cost functional L is obtained from 20 first order differential equations (31) and 24 boundary conditions (10 equations constraining the initial state, 10 equations for the final values of Lagrange multipliers and 4 equations for $\boldsymbol{\psi}$). The driving torques for manipulator joints are computed from the algebraic equation resulting from (29). The trajectory planning is performed offline before the

experiment. We use a Matlab script with bvp4c solver (a finite difference code that implements the three-stage Lobatto IIIa formula). The optimal trajectory is compared with a simple straight-line trajectory. In this reference trajectory, the end-effector velocity in the inertial reference frame is constant during the major part of the motion (1.25s is allocated for end-effector acceleration at the beginning and the same amount of time is allocated for reducing the end-effector velocity to zero). This straight-line trajectory is used as an initial guess of the solution of the BVP problem. Both the straight-line and the optimal trajectories defined in the Cartesian space are transferred to the velocities of manipulator joints. During the experiment, joint controllers were used to assure trajectory realization in the configuration space and there was no feedback from the measurement of the end-effector position.

The reference end-effector trajectory in the Cartesian space and the results of the experiment (i.e. positions of the end-effector measured by the visual pose estimation system) are presented in Fig. 2 (on the XY plane), in Fig. 3 and Fig. 4. The difference between the reference end-effector position and the end-effector position measured by the visual pose estimation system is shown in Fig. 5. It can be seen that for both trajectories the end-effector position obtained from the experiment is very close to the planned reference trajectory (the error is less than 0.015m after 5s of motion). Fig. 6 shows four frames from a video recorded during the realization of the optimal trajectory on the planar air-bearing microgravity simulator. The change of the satellite orientation, clearly visible in this figure, is caused by reaction torques and reaction forces induced by the motion of the manipulator. The free-floating nature of the satellite-manipulator system was taken into account during trajectory planning with equations presented in Section 2. Thus, the end-effector follows the desired trajectory despite the changes in satellite orientation. Finally, in Fig. 7 and Fig. 8, the reference positions of the manipulator joints during the realization of both trajectories are presented. Additionally, driving torques that should be applied in the manipulator joints are also presented in these two figures. The initial positions of the manipulator joints for both the straight-line and the optimal trajectories are the same (initial conditions were exactly the same for both experiments). In the presented case, the final position of the manipulator joints are also almost identical for the straight-line and the optimal trajectories (the difference is less than 0.1 degrees for both joints). The initial and final torques in the optimal trajectory are non-zero, but there is no boundary condition that would require zero control torques. Three phases of the straight-line trajectory (end-effector acceleration, motion with constant velocity and breaking) are reflected in control torques. The optimization algorithm (with the selected quadratic norm of the control input as a cost functional) resulted in smoother behaviour of the control input. Here it should be noted that in the test set-up the DC motors move the manipulator joints though harmonic drives, while in our computations the gear reduction ratio is not taken into account. The optimization procedure allowed for 60.2% reduction of the cost functional connected with the power use of the manipulator motors.

To more thoroughly assess what the advantage of using the optimization method over utilization of a simple straight-line trajectory is, we analysed 30 trajectories based on randomly selected initial and final end-effector positions. The area in which the end-effector positions were selected was limited to a rectangle defined by apexes: $\mathbf{P}_A = [0.4m\ 0.2m]^T$ and $\mathbf{P}_B = [1.0m\ 0.8m]^T$ (expressed in the inertial reference frame located at the initial position of the manipulator-equipped satellite centre of mass). The time of motion was set to 4s. All other parameters were the same as in the presented experimental example. For each pair of points, a straight-line trajectory was constructed and then used as an initial guess solution for the BVP problem. The cost functional L (quadratic norm of the control input) was calculated for each straight-line and optimal trajectory. The performed study found that for these randomly selected 30 pairs of points, the average reduction of the cost functional resulting from the trajectory optimization was 49.4%, while the lowest obtained reduction of L was 19.67%.

Table 1: Properties of the planar satellite-manipulator.

	Parameter	Value
1	Satellite mass	12.9 kg
2	Satellite moment of inertia	0.208 kg·m^2
3	Position of manip. mounting ($\mathbf{r}_q$)	[0.327 0] m
4	Manipulator link 1 mass	4.5 kg
5	Manipulator link 1 moment of inertia	0.32 g·m^2
6	Manipulator link 1 length	0.62 m
7	Manipulator link 2 mass	1.5 kg
8	Manipulator link 2 moment of inertia	0.049 kg·m^2
9	Manipulator link 2 length	0.6 m

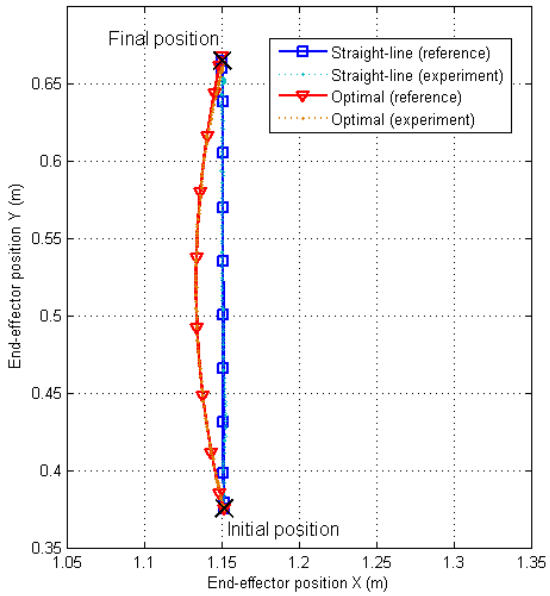

Figure 2: End-effector position on XY plane (straight-line vs optimal).

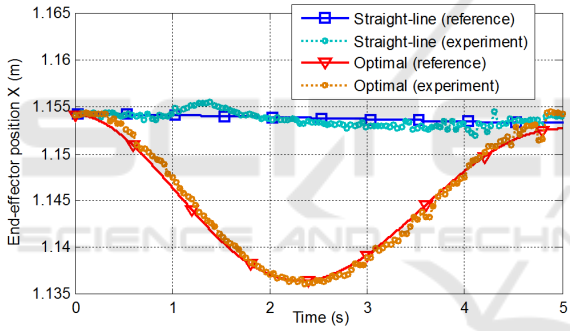

Figure 3: X-component of the end-effector position (straight-line vs optimal).

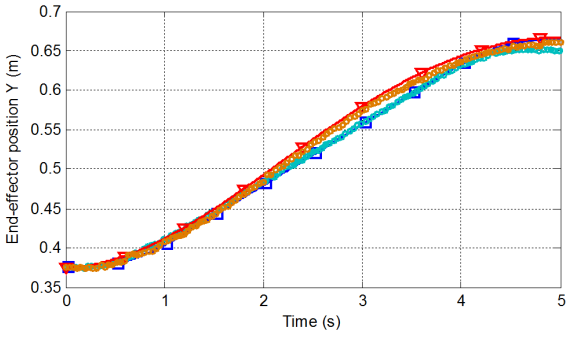

Figure 4: Y-component of the end-effector position (straight-line vs optimal).

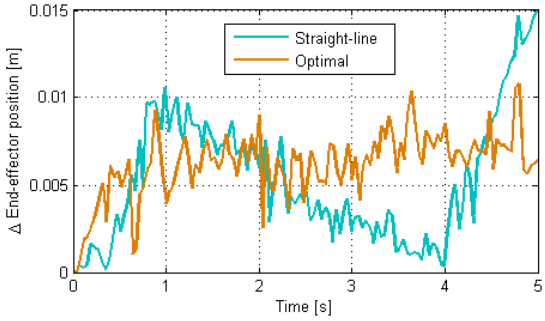

Figure 5: Difference between the reference end-effector position and position measured during experiment.

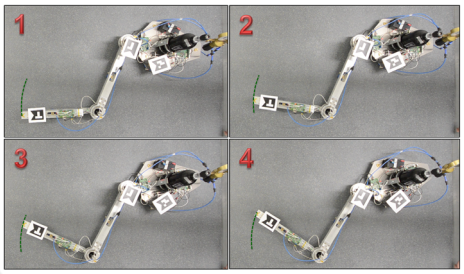

Figure 6: Planar satellite-manipulator system during realization of the optimal trajectory on the air-bearing microgravity simulator.

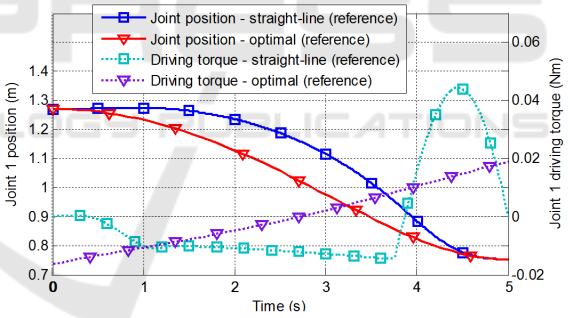

Figure 7: Reference position of manipulator joint 1 and driving torque applied in this joint (straight-line vs optimal).

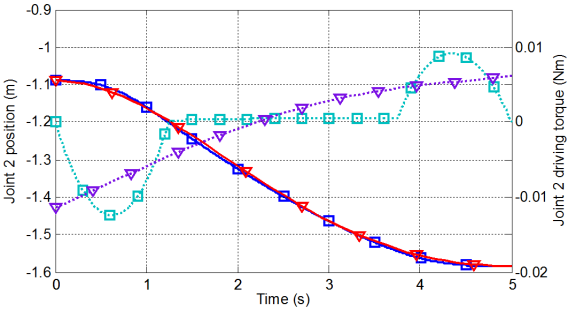

Figure 8: Reference position of manipulator joint 2 and driving torque applied in this joint (straight-line vs optimal).

5 APPLICATION OF THE OPTIMIZATION ALGORITHM FOR A MANIPULATOR WITH 4 DEGREES OF FREEDOM

In this section we present the results of trajectory optimization performed for the WMS1 LEMUR (Seweryn et al., 2014). A picture of this manipulator is presented in Fig. 9, while Tab. 2 summarizes its basic properties. It is a manipulator with 7 degrees of freedom. However, we perform trajectory optimization only for the first four joints. The driving torques required for the positioning of the end-effector are higher than the driving torques required for obtaining the desired orientation of the end-effector. For the manipulator with 7 degrees of freedom we present results of numerical simulations only. For the system with a manipulator with 4 degrees of freedom the solution that minimizes L is obtained from 40 first order differential equations and 46 boundary conditions (20 equations constraining state at t_0, 20 equations for $\boldsymbol{\lambda}_{vp}$ at t_f and 6 equations for $\boldsymbol{\psi}$).

The initial position of the end-effector (expressed in CS_{ine} located at the initial position of the servicing satellite centre of mass) is $\mathbf{r}_{ee}(t = t_0) = [0.8m \;\; -0.1m \;\; 0.4m]^T$, while the desired final end-effector position is $\mathbf{r}_{ee}(t = t_f) = [0.8m \;\; -0.1m \;\; 0.6m]^T$. The initial and final velocity of the end-effector is zero. There is no initial velocity of the servicing satellite. The desired time of motion is $4s$. As in the case of the planar system, we use a straight-line trajectory as the initial guess for the BVP solution and for comparison with the optimal trajectory. The straight-line trajectory is divided into a $2s$ phase of end-effector acceleration (in CS_{ine}) and a $2s$ phase of breaking. The position and velocity of the end-effector for both trajectories are presented in Fig. 10 and Fig. 11. The positions of first four manipulator joints are presented in Fig. 12, while torques applied on these joints are shown in Fig. 13. In this example the driving torques required for the realization of both trajectories are far lower than the maximal available driving torques ($15Nm$).

The optimization algorithm allowed 68% reduction of the cost functional L (from $L_{str} = 11.4$ to $L_{opt} = 3.56$). Although the final end-effector position differs from the initial end-effector position only by Z-component, in Fig. 8 it can be seen that all components of the end-effector position changed during the realization of the optimal trajectory (X- and Y-components return to their initial values at the end). The boundary condition sets the final end-effector velocity to zero - this is the main advantage of the modified algorithm in comparison to its previous version presented by Seweryn and Banaszkiewicz (2008). No condition is set on the final velocities of the manipulator joints. Thus, in the considered case the final velocities of the manipulator joints are not equal to zero.

Table 2: Properties of the spatial satellite-manipulator.

	Parameter	Value
1	Satellite mass (assumed)	100 kg
2	Satellite moment of inertia	diag([2.8 6.1 7.4]) kg·m^2
3	Number of manip. joints	7
4	Total length of manipulator	3.1 m
5	Total mass of manipulator	15.25 kg
6	Maximal joint driving torque	15 Nm

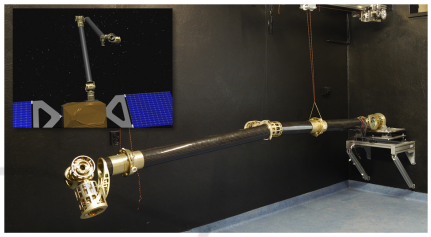

Figure 9: Prototype of the WMS1 LEMUR robotic arm and visualization of this manipulator on a servicing satellite.

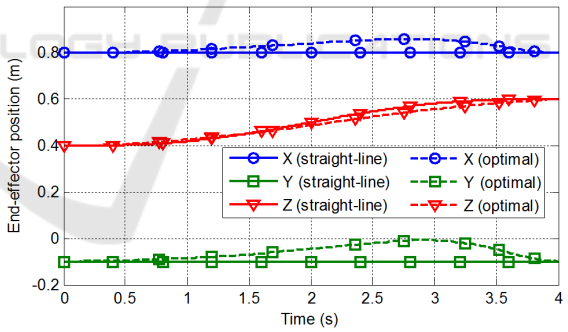

Figure 10: End-effector position (straight-line vs optimal).

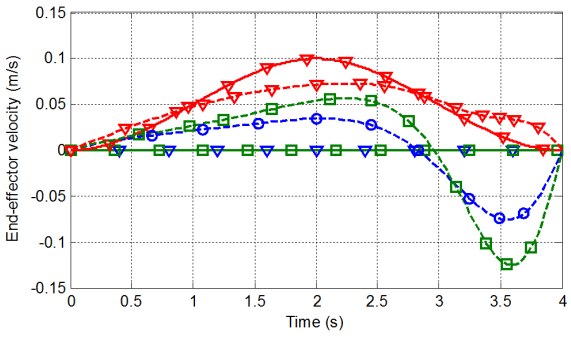

Figure 11: End-effector velocity (straight-line vs optimal).

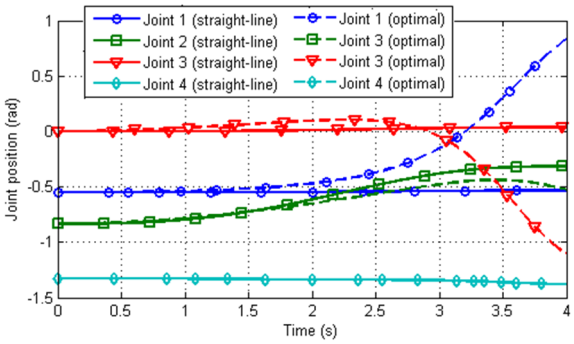

Figure 12: Positions of manipulator joints (straight-line vs optimal).

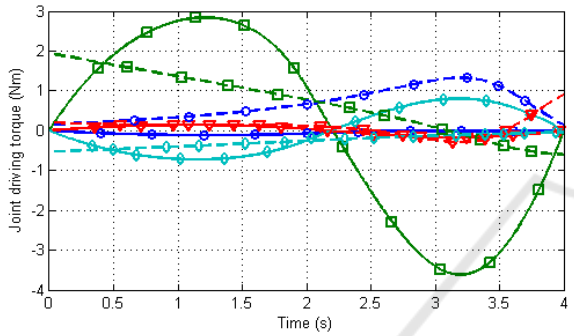

Figure 13: Driving torques at manipulator joints (straight-line vs optimal).

6 DISCUSSION

The use of the trajectory optimization algorithm for free-floating satellite-manipulator systems was demonstrated for two cases: (i) a planar system with a manipulator with 2 degrees of freedom and (ii) a spatial system with a manipulator with 4 degrees of freedom (with four joints responsible for obtaining desired end-effector position). In the first case the experiments were performed on the planar air-bearing microgravity simulator. In the second case, only numerical simulations were performed, but the mass and geometrical properties of a real prototype of a space manipulator were used.

As in the approach presented by Seweryn and Banaszkiewicz (2008) quadratic norm of the control input has been used as a cost functional that was minimized. Such approach is simple and common in automation and robotic. The presented method could be modified by using a more complex cost functional that would, e.g., minimize changes in the satellite orientation. In each case the optimal trajectory was compared with a straight-line trajectory and it was proven that the optimization algorithm allows for substantial reduction of the power use of the manipulator motors. Moreover, for the planar case the analysis was performed with 30 trajectories based on randomly selected initial and final end-effector position and it was found that the average reduction of the selected cost functional resulting from the trajectory optimization was 49.4%. In all presented cases the required driving torques for the manipulator joints were far lower that the maximal available control torques. However, it is expected that in the rigidization and detumbling phases after the orbital capture manoeuvre the required driving torques will be higher, as the large mass of the target object will be attached to the end-effector. In such a case, the presented optimization method may prove to be very useful.

There are two main weaknesses of the presented optimization algorithm: (i) it is not guaranteed that the global minima will be found, and (ii) the computational cost of the trajectory optimization is very high. The second issue could be especially problematic in case of algorithm implementation on flight hardware. However, the trajectory planning stage can be performed while the manipulator-equipped satellite is waiting in a safe point (it might even be possible to perform such computations on Earth).

Current work focuses on selecting more practical cost functional (e.g., to achieve minimization of the manipulator influence on the satellite) and performing trajectory optimization after the grasping of the target object. Precise evaluation of algorithm computational cost is also currently performed.

7 CONCLUSIONS

Manipulator trajectory planning is important for planned active debris removal and on-orbit servicing missions. The successful demonstration of the trajectory optimization algorithm on the experimental test set-up (the planar air-bearing microgravity simulator) was an important step in the development of this algorithm. The simulations performed for the spatial manipulator with 4 degrees of freedom with mass and geometrical properties of the prototype robotic arm (WMS1 LEMUR) were also useful for the algorithm validation. Thus, the results presented in this paper serve not only as an illustration and example of the optimization algorithm application, but allow as an assessment of the possibility of using trajectory optimization during one of the planned active debris removal and on-orbit servicing missions.

ACKNOWLEDGEMENTS

This paper was partially supported by The National Centre for Research and Development project no. PBS3/A3/22/2015.

REFERENCES

Aghili, F. (2008) 'Optimal control for robotic capturing and passivation of a tumbling satellite with unknown dynamics', *AIAA Guidance, Navigation, and Control Conference and Exhibit (AIAA-GNC'2008)*. Honolulu, Hawaii, USA, 18-21 August.

Dubowsky, S., Papadopoulos, E. (1993) 'The kinematics, dynamics, and control of free-flying and free-floating space robotic systems', *IEEE Transactions on Robotics and Automation*, 9(5), pp. 531-543.

Flores-Abad, A., et al., (2014a) 'Optimal Control of Space Robots for Capturing a Tumbling Object with Uncertainties', *Journal of Guidance, Control, and Dynamics*, 37(6), pp. 2014-2017.

Flores-Abad, A., et al. (2014b) 'A review of space robotics technologies for on-orbit servicing', *Prog. Aerosp. Sci.*, 68, pp. 1-26.

Hausmann, G., et al. (2015) 'E.Deorbit Mission: OHB Debris Removal Concepts', *13th Symposium on Advanced Space Technologies in Robotics and Automation (ASTRA'2015)*. Noordwijk, The Netherlands, 11-13 May.

Junkins, J.L., Schaub, H. (1997) 'An Instantaneous Eigenstructure Quasivelocity Formulation for Nonlinear Multibody', *Dynamics. J. Astronaut. Sci.*, 45(3), pp. 279-295.

Kaigom, E. G., Jung, T. J., Rossmann, J. (2011) 'Optimal Motion Planning of a Space Robot with Base Disturbance Minimization', *11th Symposium on Advanced Space Technologies in Robotics and Automation (ASTRA'2011)*. Noordwijk, The Netherlands, 12-14 April.

Lindberg, R. E., Longman, R. W., Zedd, M. F. (1993) 'Kinematic and dynamic properties of an elbow manipulator mounted on a satellite', in Xu, Y., Kanade, T. (eds.) *Space Robotics: Dynamics and Control*. New York: Springer.

Liou, J.-C., Johnson, N.L., Hill, N.M. (2010) 'Controlling the growth of future LEO debris populations with active debris removal', *Acta Astronautica*, 66 (5-6), pp. 648 - 653.

Rybus ,T., Seweryn, K. (2015) 'Manipulator trajectories during orbital servicing mission: numerical simulations and experiments on microgravity simulator', *6th European Conference for Aeronautics and Space Sciences (EUCASS'2015)*. Kraków, Poland, 29 June -2 July.

Rybus, T., Seweryn, K., Sąsiadek, J. Z. (2016) 'Trajectory Optimization of Space Manipulator with Non-zero Angular Momentum During Orbital Capture Maneuver', *AIAA Guidance, Navigation, and Control Conference (AIAA-GNC'2016)*. San Diego, California, USA, 4-8 January.

Rybus, T., et al. (2013) 'New Planar Air-bearing Microgravity Simulator for Verification of Space Robotics Numerical Simulations and Control Algorithms', *12th Symposium on Advanced Space Technologies in Robotics and Automation (ASTRA'2013)*. Noordwijk, The Netherlands, 15-17 May.

Seweryn, K., Banaszkiewicz, M. (2008) 'Optimization of the Trajectory of a General Free-Flying Manipulator During the Rendezvous Maneuver', *AIAA Guidance, Navigation, and Control Conference and Exhibit (AIAA-GNC'2008)*. Honolulu, Hawaii, USA, 18-21 August.

Seweryn, K., et al. (2014) 'The laboratory model of the manipulator arm (WMS1 LEMUR) dedicated for on-orbit operation', *12th International Symposium on Artificial Intelligence, Robotics and Automation in Space (i-SAIRAS'2014)*. Saint-Hubert, Quebec, Canada, 17-19 June.

Shah, S. V., et al. (2013) 'Energy optimum reactionless path planning for capture of tumbling orbiting objects using a dual-arm robot', 1st International and 16th National Conference on Machines and Mechanisms (iNaCoMM'2013). IIT Roorkee, India, 18-20 December.

Sullivan, B., Akin, D. (2012) 'Satellite servicing opportunities in geosynchronous orbit', *AIAA SPACE 2012 Conference and Exposition*. Pasadena, California, USA, 11-13 September.

Umetani, Y., Yoshida, K. (1989) 'Resolved motion rate control of space manipulators with generalized jacobian matrix', *IEEE Transactions on Robotics and Automation*, 5 (3), pp. 303-314.